*AAPS PharmSciTech, Vol. 19, No. 3, April 2018 (© 2018)*
DOI: 10.1208/s12249-017-0949-0

*Research Article*

# Facile Synthesis of Chitosan Capped Mesoporous Silica Nanoparticles: A pH Responsive Smart Delivery Platform for Raloxifene Hydrochloride

**Priya V. Shah[1] and Sadhana J. Rajput[1,2]**

*Received 13 October 2017; accepted 28 December 2017; published online 16 January 2018*

***Abstract.*** An encapsulation of model drug raloxifene hydrochloride (RAL) inside the chitosan decorated pH responsive mesoporous system has a greater potential for accumulating in the tumor cells. The present study involves synthesis of surface modified mesoporous silica nanoparticles (MSN) with the aim of achieving pH sensitive drug delivery system. A silanol skeleton of MSN has been productively modified to amine intermediate which served as a firm platform to adapt chitosan grafted assembly and systematically evaluated. RAL incorporation inside the featured mesopores was performed employing novel immersion solvent evaporation methodology and evaluated further. The pH responsive behavior of formulated nano framework was studied at three different pH of a phosphate buffer saline individually. The *in vitro* cell viability assay on MCF-7 breast carcinoma cells was performed in time and concentration dependent manner. Finally, the hemolysis assay of designed nanoparticle was accomplished to envisage the hemocompatibility. The outcome of characterization details unveiled a perfect 2D hexagonal spherical structure gifted with higher surface area and optimum pore size for designed nanoparticles. The higher percentage grafting of amine and chitosan residue, *i.e.*, 4.01 and 28.51% respectively along with 31.89 and 33.57% RAL loading efficiency made MSNs more attractive and applicable. Eventually, *in vitro* release study exhibited higher RAL release in acidic media for extended time periods confirming successful formation of pH responsive nanoparticle having controlled release property. Conclusively potential of designed nanosystem to serve efficient anti-cancer remedy was confirmed by superior behaviour of chitosan grafted MSN towards MCF-7 cells with supreme hemocompatibility.

**KEY WORDS:** raloxifene hydrochloride; anomalous release; chitosan; MCF-7; hemolysis assay.

## INTRODUCTION

Cancer is exerting a greater impact on the global health as its worldwide incidences are continuingly rising every year. It involves an uncontrolled growth of cells, which can invade and spread to distant sites of the body. Breast, lung, prostate, colorectal, stomach, uterine cervix, and liver cancer are the most common types of cancer (1). The most common treatment involves use of chemotherapeutic moieties as a remedy to fight cancer. However, on many occasions effective output is not achieved using this approach as well. The probable reasons could be attributed to the lesser availability of active component at the tumor site, lack of specificity, selectivity, and various others (2).

Nanotechnology has created a new gateway for solving many of the biopharmaceutical and clinical limitations of conventionally available formulations. It firmly deals with the concept of overcoming the aforementioned obstacles by designing stable and biocompatible formulations which impart maximum efficacy with minimum usage and least adverse effect as well (3). Various nanoparticles (NPs) are being engineered to fulfill wide-ranged miscellaneous goals with respect to solubility enhancement, bioavailability enhancement, and tissue/organ specificity along with promising outcomes concerning stability, biocompatibility, and biodegradation (4).

Miscellaneous applications of mesoporous silica nanoparticle (MSNs) in pharma field have created a new era of nanoscience in formulation development. Furthermore, MSNs are gaining attention due to their unique and extraordinary properties like, high surface area, uniform pore size, distinctive honeycomb channeled structure, noteworthy loading and entrapment capacity, zero premature release (4,5). In the initial

**Electronic supplementary material** The online version of this article (https://doi.org/10.1208/s12249-017-0949-0) contains supplementary material, which is available to authorized users.

[1] Faculty of Pharmacy, Centre of Relevance and Excellence in New Drug Delivery System, Government of India, The Maharaja Sayajirao University of Baroda, Kalabhavan Campus, Vadodara, 390002, India.

[2] To whom correspondence should be addressed. (e–mail: sjrajput@gmail.com)

stage, it was used for the purpose of solubility enhancement in pharmaceutical field (6,7). However, with the new exploration, its applications has also widen in the field of bioavailability enhancement of poorly soluble drugs, formulating a controlled drug delivery system and for the targeting of active pharmaceutical candidates to the site of interest. In the last few years, drug accumulation inside the tumor cell by stimuli (pH, temperature, redox responsive) and receptor based concentration has gained a lot of attention (8). This could become possible through the surface modification of silanol groups by attachment of various moieties. Availability of silanol basic skeleton provides a firm platform to amend MSNs into highly effective surface decorated nanocomposites. The versatility of surface silanol groups towards ease of modification along with aforementioned remarkable properties has garnered much attention and made them NPs of choice to achieve many goals (9).

Formulating pH responsive drug delivery system is a thrust area in NPs research, which has been explored in depth in this research. pH responsive decoration of MSNs exterior involves different pH responsive ligands like chitosan (10–15), polyacrylic acid (16–18), and poly methacrylic acid (19). It is based on the concept of delivering the maximum amount of active pharmaceutical ingredient into tumor cells based on the pH difference between tumor cells and healthy cells. Wherein, tumor cells are comparatively acidic in contrast to healthy cells. Thus, surface modification by grafting pH responsive ligand may result into higher drug amassing at the tumor site (20).

This concept has been utilized in this research, taking raloxifene hydrochloride (RAL) as a model drug. It is a selective estrogen receptor modulator (SERM) having application in cancer and osteoporosis treatment (21). In spite of all the benefits associated with RAL, the effectiveness of this BCS class II drug is highly hampered by solubility limitations (22). The aim of the present work is to design a pH sensitive mesoporous silica framework with the aim of a tissue specific drug release of RAL. Herein, chitosan was selected as a pH responsive grafting molecule. The reasons behind selecting chitosan for this purpose were numerous, which include biocompatibility, nontoxicity and its biodegradable nature. One more atypical feature is presence of abundant amount of primary amine group on the outer surface. This makes chitosan freely soluble in the pH range from 1 to 11 (23,24). Furthermore, as being a polysaccharide, it controls the drug release from NPs and its extraordinary feature of swelling at lower pH made it an ideal candidate for formulating pH responsive nanoframework.

Despite of huge applications of RAL in breast cancer treatment, till now no pH responsive mesoporous formulation has been reported so far. Our group has earlier reported solubility enhancement for RAL by MSNs (25). The results obtained in this regard were encouraging. Chitosan coated MSNs exhibited a higher accumulation inside the tumor cell as compared to plain RAL and RAL encapsulated uncoated MSN, *i.e.*, RAL-41. Percent cumulative RAL release from RAL-CHITO-41 showed promising results in phosphate buffer saline solution (PBS) having pH 5.6 as compared with pH 7.4. Thus, our findings displayed more RAL release at the acidic pH of the diffusion media and it could be stated that the formulated drug delivery system could efficiently be utilized for localization of RAL in tumor cell based on the same principle.

## EXPERIMENTAL SECTION

### Materials

RAL ($\geq 99\%$) was kindly gifted by Zydus research centre, Gujarat, India. Various basic ingredients utilized in synthesis of MSN, *i.e.*, tetra methyl ammonium hydroxide pentahydrate (TMAOH; $\geq 98\%$), amorphous fumed silica ($SiO_2$; $\geq 98.5\%$, pharmaceutical grade), cetyl trimethyl ammonium bromide (CTAB; $\geq 99\%$), (3-aminoproyl) triethoxysilane (APTES), and chitosan (low molecular weight grade) were purchased from Sigma Aldrich (St. Louis, USA). Analytical grade methanol (MeOH $\geq 99\%$) and toluene ($\geq 99\%$) were obtained from Fisher Scientific (Vadodara, Gujarat). Deionized water was used in synthesis of MSNs. Moreover, standard chemicals and reagents required in diffusion media preparation like disodium hydrogen phosphate, sodium chloride and potassium dihydrogen ortho phosphate were purchased from Loba Chemie (Mumbai, Maharashtra). The cell viability assay was carried out on human breast carcinoma cell line MCF-7, which was procured from National centre for cell science (NCCS, Pune, India) and the cells were cultured in Dulbecco's modified eagle medium (DMEM) media supplemented with 0.1% penicillin and streptomycin solution and 10% fetal bovine serum (FBS) and these were purchased from Himedia laboratories. Cell culture grade dimethyl sulphoxide (DMSO $\geq 99\%$) was procured from Himedia laboratories.

### Synthesis of MSN-41

The synthesis of an initial mesoporous framework was carried out based on the Stober method with minor modifications (26). In an outline, a sequential incorporation of CTAB, TMAOH, silica and water to get a thick gel carrying a composition of 1 $SiO_2$: 0.27 CTAB: 0.19 TMAOH: 40 $H_2O$ was done. Continuous stirring for a couple of hours (h) followed by hydrothermal treatment for 48 h at 373 K in Teflon coated autoclave resulted into silica NPs with surfactant (CTAB) still intact within the pores (CTAB@MSN). Removal of surfactant was carried out by calcination of asynthesized product for 5.5 h at 823 K in a muffle furnace. The obtained product was labeled as MSN-41.

### Synthesis of Amine-Attached MSN

Amine modified MSNs were synthesized via post synthetic grafting approach with few modification (27,28). Wherein, 0.1 g (g) MSN-41 were dispersed in 25 mL of dried toluene, followed by subsequent addition of 1.38 mL of APTES and refluxing the reaction mixture at 120°C for 24 h. The acquired material was labeled as MSN-$NH_2$-41. Then after, the obtained slurry was filtered and given the excessive wash with toluene and product was collected after vacuum drying (Fig. 1).

### Synthesis of Chitosan-Capped MSN

Chitosan grafting on MSN-41 was carried out as per earlier reported method (10). Twenty-five milligrams chitosan was dissolved in 5 mL of 3% acetic acid and the suspension was

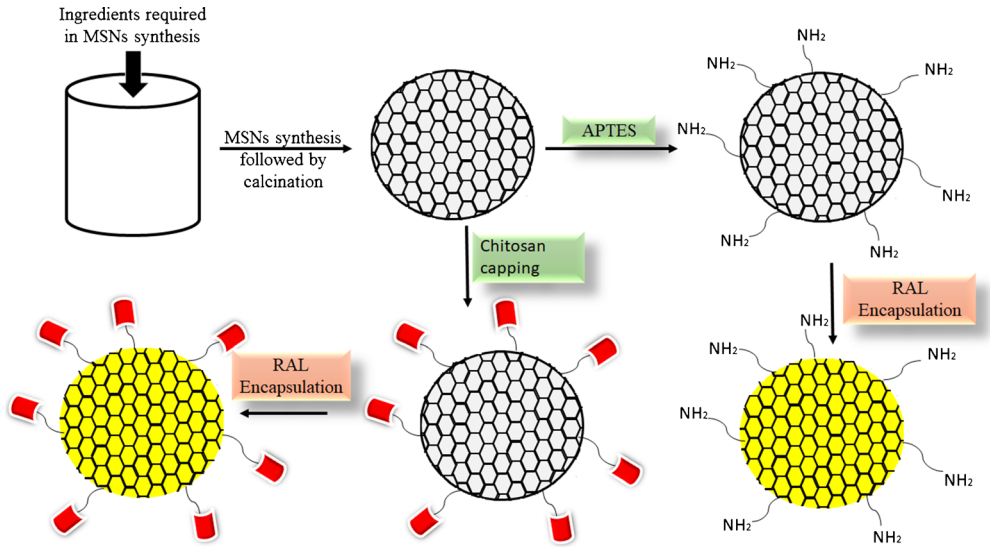


**Fig. 1.** Schematic representation of synthesis of MSN-CHITO-41

stirred at 600 rpm for 24 h to form a chitosan solution (0.5%*w/v*). Subsequently, dispersion of 10 mg of bare MSN-41 in 5 mL of MeOH was prepared and pH of the dispersion was adjusted between 3.5 and 4.5 using acetic acid. The reaction assembly for stirred vigorously subsequent to incorporation of 200 µL of APTES at room temperature (RT). Eventually, 5 mL chitosan solution was added to above dispersion and stirred at RT for 24 h. The chitosan-coated MSN were collected by centrifugation at 10000 rpm, following excessive washing with distilled water and methanol before freeze drying and labeled as MSN-CHITO-41. Overall schematic representation of MSN-41 to MSN-CHITO-41 is displayed in Fig. 1.

## Estimation of Amine and Chitosan Group Grafted on the Surface of MSN-41

### *Quantification of %Amine Attachment*

*Quantification by Ninhydrin Assay.* Estimation of amine group attached on the surface of MSN-41 and the degree of grafting was performed by Ninhydrin colorimetric assay (29,30). The basic principle behind this method involves reaction between ninhydrin reagent and surface amine residues of MSN-$NH_2$-41 that gives color product, which was efficiently analyzed by colorimetric method at 590 nm. To quantify the surface decorated amine groups, a calibration curve of absorbance *versus* concentration was generated taking APTES as a standard in the concentration range of 0.1 to 0.5 µM. Where, appropriate amount of APTES was transferred to a solution containing sodium acetate/acetic acid buffer followed by subsequent addition of 2 mL of 2% ninhydrin reagent and the reaction mixture was heated at 78°C for 10 min and cooled to RT. This was succeeded by methanol incorporation to obtain final volume of 10 mL. The entire solution was centrifuged and the supernatant was taken and designated as V (L) followed by UV-VIS spectrophotometric analysis. A similar procedure was followed by taking the required amount (W, g) of MSN-$NH_2$-41 and concentration of amine group was calculated from the regression equation generated from the calibration plot. Other parameters, for instance, the amount of grafted amine groups ($A_m$) (mol/g), number of amine molecules ($A_n$) (molecule/$nm^2$), the weight percentage of amine group ($\%W_a$) etc. were calculated using the following equations (31).

$$A_m\left(\frac{\text{mol}}{\text{g}}\right) = \frac{MV}{W} \tag{1}$$

$$A_n\left(\text{molecule/nm}^2\right) = \frac{A_m}{\text{SA}} \times 6.02 \times 10^5 \tag{2}$$

$$\%W_a = A_m \times M_{ap} \times 100 \tag{3}$$

Where,

| | |
|---|---|
| $M$ | corresponding concentration of amino group (g/mol) |
| $V$ | volume of supernatant obtained after centrifugation (L) |
| $W$ | initial amount of MSN-$NH_2$ taken (g) |
| SA | BET surface area ($m^2$/g) |
| $M_{ap}$ | molecular weight of aminopropyl group. |

*Quantification by Thermal Method.* Herein, pristine MSN-41 and MSN-$NH_2$-41 were exposed to thermal gravimetric treatment to 700°C keeping heating rate of 5°C/min. %Weight loss was calculated and %attachment were calculated in terms of %weight gain using following Eq. 4 (32):

$$\%W_{AMINE} = \%W_{\text{MSN-NH}_2\text{-41}} - \%W_{\text{MSN-41}} \tag{4}$$

### *Estimation of % Chitosan Grafted on the Surface of the MSN-$NH_2$*

An identical approach was adopted for calculation of %weight of chitosan grafted on the external surface as followed for the calculation of amine residue grafted on the surface of MSN-$NH_2$-41. Unmodified MSN and MSN-CHITO-41 were analyzed by the TGA and %weight losses for the same were

calculated and designated as $\%W_{\text{MSN-41}}$ and $\%W_{\text{MSN-CHITO-41}}$. The %weight of chitosan ($\%W_{\text{CHITO}}$) is calculated using the following equation.

$$\%W_{CHITO} = \%W_{\text{MSN}-CHITO-41} - \%W_{\text{MSN}-41} \quad (5)$$

### Preparation of RAL-Loaded MSNs

A unique immersion-solvent evaporation method was followed to formulate RAL-loaded MSNs. This method involved preparation of highly concentrated RAL solution in MeOH followed by addition of NPs (mass ratio 1:1.5). This reaction assembly was kept under stirring for 1 h. Sequentially, it was subjected to rotary evaporation treatment. Subsequently, the product was vacuum dried. RAL occupied NPs were assigned RAL-41, RAL-$NH_2$-41, and RAL-CHITO-41 for MSN-41, MSN-$NH_2$-41, and MSN-CHITO-41 respectively. %Drug loading capacity and %entrapment efficiency was calculated by the UV spectrometric method analyzed at a wavelength maxima of 285 nm using following equation.

$$\%\textit{Entrapment Efficiency} = \frac{\textit{Total weight of RAL present in nanoparticles}}{\textit{Weight of RAL added initially}} \times 100 \quad (6)$$

$$\%\text{Loading Efficiency} = \frac{\text{Total weight of RAL present in nanoparticles}}{\text{Total weight of drug loaded nanoparticles}} \times 100 \quad (7)$$

%Loading efficiency was further confirmed by TGA analysis of the drug incorporated NPs. TGA analysis for the plain drug (RAL), RAL-41, RAL-$NH_2$-41, and RAL-CHITO-41 were performed keeping temperature up to 700°C with the rate of 5°C/min. Graph of %weight loss *versus* temperature (°C) was plotted to acquire percentage loading details.

### Solid State Evaluation of Plain and RAL-Loaded MSN-41, MSN-$NH_2$-41, and MSN-CHITO-41

Formation of MSNs and confirmation of RAL loading inside the pores was done by FT-IR analysis of plain MSN-41, MSN-$NH_2$-41, MSN-CHITO-41, and drug-encapsulated MSNs, i.e., RAL-41, RAL-$NH_2$-41, and RAL-CHITO-41. Complete analysis was carried out using Bruker ALPHA-T instrument with spectral analysis ranging from 4000 to 600 $cm^{-1}$. The crystalline behavior and complete encapsulation of drug into NPs was evaluated by small and wide angle X-ray diffraction (SAXS/WAXS) performed on EMPYREAN, PANalytical model operated at 40 kV and 30 mA and equipped with Cu Ka radiation beam. The SAXS and WAXS pattern were recorded in the 2θ/° ranging from 0.5° to 10° and 10° to 40° with a scan rate of 0.02°/min and 0.03°/min, respectively. Furthermore, morphological evaluation was accomplished by scanning electron microscope (SEM) equipped with elemental analyzer operated at an acceleration voltage of 15 kV. Subsequently, microscopical investigation was done on transmission electron microscope (TEM) using TEM CM 200 (Philips, India) model operated at 200 kV voltage with resolution of 2.4 A°. Nitrogen desorption analysis was executed on Micromeritics ASAP 2020 instrument to record atypical hysteresis loop resulting type IV isotherm under −196°C temperature and *Brunauer–Emmett–Teller* (BET) surface area, Barrett-Joyner-Halenda (BJH) surface area, BJH pore size, and pore volume were calculated. Eventually, thermal analysis was accomplished on Shimadzu DSC60 model equipped with TA 60-WS software to confirm absence of extra drug present on the external surface of NPs which confirms complete entrapment of RAL within the carrier. The success of amine attachment and chitosan grafting was investigated by dynamic light scattering (DLS) analysis where the zeta potential for each NPs were recorded on MALVERN zeta sizer version 6.20. Wherein, NPs were dispersed in deionized water and sonicated for 5 min followed by DLS analysis.

### *In vitro* Release Study

The pH responsive behavior of formulated RAL-CHITO-41 was studied by performing *in vitro* release study in PBS buffer having three different pH (PBS: 5.6, 6.8, and 7.6). Ten milligrams plain RAL was dispersed in 5 mL diffusion media and acquired dispersion was filled in dialysis bag. Subsequently, sealed bag was immersed into 100 mL diffusion media. The entire assembly was kept at 37°C temperature and rotated at the speed of 75 rpm. Aliquots were withdrawn at predefined time interval and it was replenished by an equivalent volume of fresh diffusion medium up to 72 h. Eventually, %cumulative drug release (%CDR) was calculated and the release pattern for RAL at different pH was studied. Identical procedure was adopted to study release pattern of RAL for uncoated and polymer coated NPs wherein the formulation equivalent to 10 mg of RAL was dispersed in diffusion media.

### Release Kinetics Study

RAL release from different NPs was evaluated to study the release kinetic behavior. The cumulative drug release data were fitted to four different kinetic models viz., zero order, first order, Higuchi and Korsmeyer-Peppas model (33). In order to get best the fit mathematical model, regression coefficient value ($R^2$) and Akaike Information Criterion (AIC). These two parameters were selected and the model with highest $R^2$ value and lowest AIC value was declared to be the best fit model. Moreover, to study the release mechanism, $n$ value of Korsmeyer-Peppas model was calculated. The formulation exhibiting n value $\leq 0.45$ is follows Fickian diffusion mechanism where a single system plays a vital role in diffusion. Whereas, the formulation showing $n$ value between 0.45 and 1 is termed as the system is following non-Fickian or anomalous release mechanism where release is controlled by two individual systems concurrently.

### Estimation of Cell Viability Assay

Cell viability studies of the formulated NPs and plain NPs (without RAL) were performed by MTT assay carried out on human breast carcinoma cell line, *i.e.*, MCF-7 cell line. The first step of the MTT assay is *seeding*. Where, the cells were cultured in the 96-well plates using DMEM containing

sodium pyruvate, L-glutamate, sodium bicarbonate along with high glucose supplemented with 10% fetal bovine serum (FBS) and 1% penicillin-streptomycin (Pen/strep) solution which resist bacterial growth. One hundred microliters cell suspension was added to each well (10,000 cells/well) followed by incubation at 37°C for 24 h in incubator. Seeding step was followed by most crucial step, *i.e.*, the *drug treatment* step. Wherein, formulation containing 1-8 μM equivalent RAL and bare and surface coated NPs in the range of 0.1–100 μM were added and eventually well plate was incubated for a desired period time (24 and 72 h). Lastly, cells were given MTT dye treatment which was followed by plate reading at 570 nm. To nullify the false negative results, a negative control (cells left with drug treatment) and blank (DMSO) was taken into consideration and %cell viability was calculated by below Eq. 8.

$$\%Cell\ Viability = \frac{O.D._{.sample} - O.D._{.blank}}{O.D._{.negative\ control} - O.D._{.blank}} \times 100 \quad (8)$$

### Hemolysis Assay

It was also of prime importance to study the interaction of prepared NPs with the erythrocytes to investigate the presence of any hemolytic effect (33). It was performed as per the methods available in the literature (1,34,35). Briefly, the freshly collected human blood was subjected to EDTA treatment followed by centrifugation for 5 min at 8000 rpm for the removal of plasma. The residues were rinsed with plenty of PBS buffer having pH 7.4 and diluted ten times with the same. An equal volume of the above red blood cells (RBCs) suspension (200 μL) was added to the 800 μL of the samples having a concentration ranging from 0.1–100 μg/mL. 2%*v*/*v* Triton X-100 and PBS buffer (pH: 7.4) were taken as a positive and negative control, respectively. All the samples were incubated at 37°C for the 2 h. Subsequently, the incubated samples were centrifuged at 10,000 rpm for 2 min and collected supernatant was analyzed at 540 nm by UV spectrophotometry. %Hemolytic activity for all the samples were calculated using following Eq. 9:

$$\%Hemolysis = \frac{A_{sample} - A_{Negative\ Control}}{A_{Positive\ Contol} - A_{negative\ Contol}} \times 100 \quad (9)$$

## RESULTS

### Evaluation of MSNs

FT-IR spectroscopy of pure RAL, MSNs, and RAL-MSNs composite is illustrated in supplementary Fig. 1. Figure 1 (A) displayed FT-IR spectrum of RAL with a prominent stretching vibration peak at 3490, 2930, 1605, and 1268 $cm^{-1}$ that represents phenolic –OH group, C-H group, C=O and C-O group, respectively. Figure 1 (B) revealed a sharp C-H stretching vibration noticed at 2922 and 2852 $cm^{-1}$ along with a C-H deformation vibration peak at 1454 $cm^{-1}$ which could be attributed to surfactant present inside the pores of CTAB@MSN. However, aforementioned characteristic peaks of surfactant were missing in the spectrum of MSN-41 (Fig. 1 (C)) which confirmed a complete removal of the template. Furthermore, a broad and diffused absorption peak because of stretching vibration of terminal Si-OH (silanol) group in the region of 3300–3500 $cm^{-1}$ was accompanied by symmetric and asymmetric stretching vibration peak for Si-O-Si at 1100 and 780 $cm^{-1}$ respectively further confirmed successful MSN-41 synthesis. MSN-$NH_2$-41 exhibited similar silica framework along with additional peak at 2915 and 1585 $cm^{-1}$, which was accounted for by C-H stretching and N-H bending vibration peak respectively (Fig. 1 (D)). On the other hand the O-H and N-H stretching, C-H stretching, and N-H bending peak in the region of 3379, 2907, and 1576 $cm^{-1}$ in Fig. 1 (E) is assigned to chitosan grafting on MSN-41. Besides this, characteristic peaks appearing in Fig. 1 (A) disappeared for RAL incorporated MSNs which confirmed a complete loading of RAL inside the mesopores (Fig. 1 (F-H)).

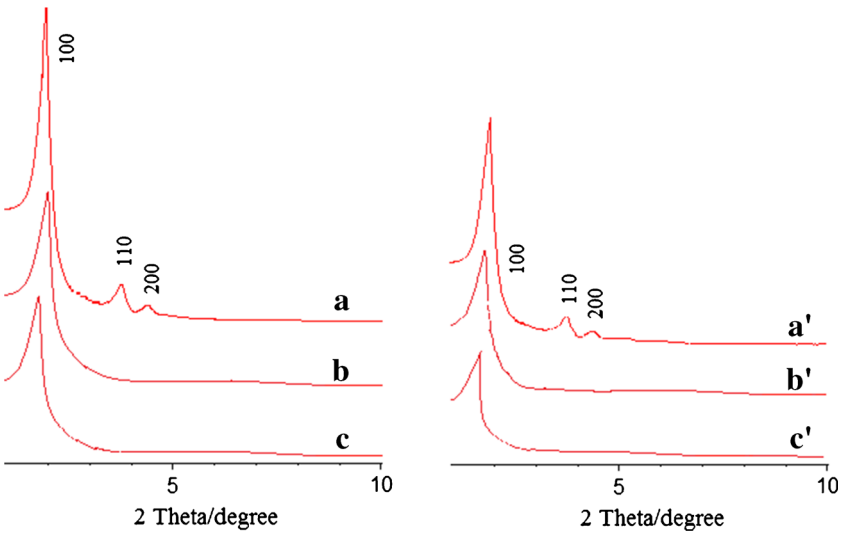


**Fig. 2.** SAXS pattern of (A) MSN-41 and (**a**') RAL-41; (**b**) MSN-$NH_2$-41 and (**b**′) RAL-$NH_2$-41; (**c**) MSN-CHITO-41 and (**c**′) RAL-CHITO-41

A typical SAXS pattern for plain and RAL loaded NPs recorded in the region of 0 to 10° 2θ/° region is portrayed in below Fig. 2. SAXS results demonstrated a prominent peaks viz., 100, 110, and 200 in the region between 1 to 10 2θ/° theta regions for MSN-41 as displayed in Fig. 2(A). Both amine modified and chitosan grafted MSNs displayed a typical peak due to mesoporous structure which demonstrate that the mesoporous framework remained unchanged even after surface modification (Fig. 2(B, C)) excluding later two peaks of 110 and 200. The intensity of these peaks would be decreases drastically and so that both could not be detected in SAXS of surface grafted MSNs. Identical conclusion was drawn for drug incorporated NPs as SAXS data which were comparable to results as obtained for plain MSNs except suppression of XRD peak (Fig. 2(A′–C′)). In other words, SAXS pattern for all NPs revealed mesoporous structure remained intact after encapsulation of RAL. Furthermore, WAXS pattern of pure RAL shown in Fig. 3(A) manifested distinct crystal diffraction peaks ranging from 10° to 40° 2θ/° region. However, this typical crystalline behavior was absent in drug containing undecorated and polymer decorated NPs which again confirmed complete uptake of RAL inside the pores of bare and surface grafted NPs. The WAXS outcomes are unveiled in Fig. 3(B–D).

Besides FT-IR and XRD analysis, a DSC analysis of plain RAL and RAL loaded MSNs was performed to support the success of RAL uptake by NPs. Preliminary DSC investigation exhibited a sharp endothermic peak at 262.06°C for RAL (Supplementary fig. 2A) and same was missing in the DSC thermograms of RAL occupied MSNs which ruled out the possibility of RAL on the external surface of MSNs (Supplementary fig. 2. B-D).

The large surface area, adjustable pore size, and pore volume are unique identity features of mesoporous framework which could be figured out by the nitrogen sorption technique. Additionally, Type IV isotherm with a hysteresis loop is a trademark of intact mesoporous structure. The specific surface area was calculated by well-known BET and BJH method, whereas BJH method was utilized for estimation of pore size. Analysis exhibited considerable high surface area for MSN-41 NPs (1141.37 $m^2$/g) which declined gradually after amine residue attachment (786.92 $m^2$/g) and further after chitosan grafting (338.47 $m^2$/g) (Fig. 4). A comparative results among drug loaded NPs and plain NPs revealed lowering of surface area following to RAL incorporation which could be attributed to RAL occupied pores as tabulated in following Table I. Besides these two parameters, another parameter namely, pore volume was

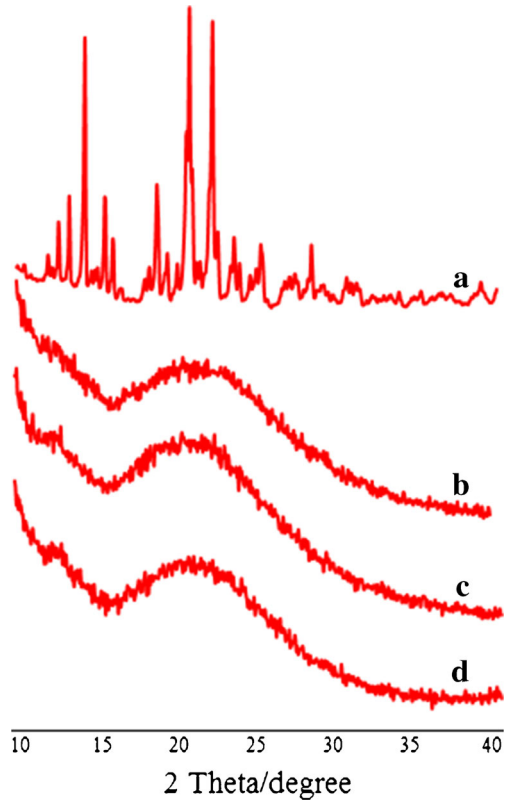


**Fig. 3.** WAXS pattern of (**a**) RAL; (**b**) RAL-41; (**c**) RAL-$NH_2$-41 (**d**) RAL-CHITO-41

obtained through BET isotherm data which showed a sharp rise at a single point, *i.e.*, at 0.68 $cm^3$/g for MSN-41-NP was equivalent to its pore volume, which could be attributed to capillary condensation of nitrogen and it is the ultimate indication of narrow and uniform particle size distribution possessing pore size of 3.69 nm (Fig. 5). Likewise, identical procedure was followed individually in detail for calculation of pore size and pore volume for different NPs and the values are summarized in Table I below.

Alternate shifting of zeta potential from negative to positive and further into more positive potential values illustrated a journey of conversion of MSN-41 to MSN-$NH_2$-41 reaching to the final destination of MSN-CHITO-41, respectively. A similar observation was drawn for RAL-41, RAL-$NH_2$-41, and RAL-CHITO-41, respectively; however, the zeta potential value was more positive in

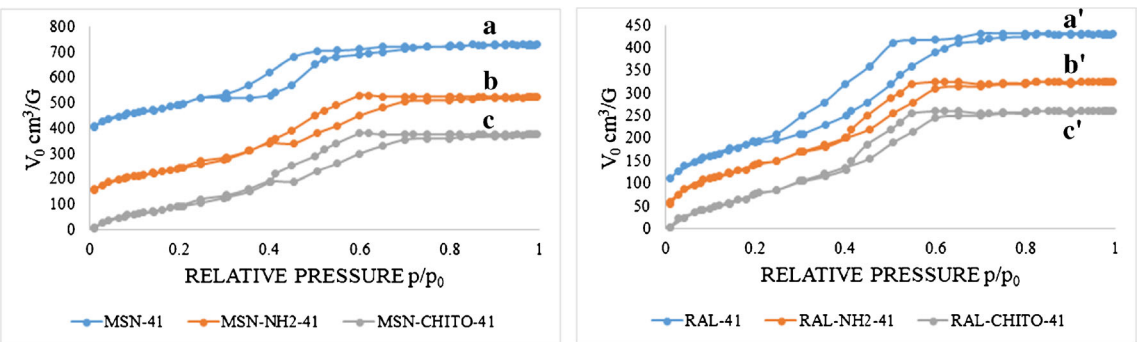


**Fig. 4.** Nitrogen adsorption-desorption graph for (**a**) MSN-41 and (**a**') RAL-41; (**b**) MSN-$NH_2$-41 and (**b**′) RAL-$NH_2$-41; (**c**) MSN-CHITO-41 and (**c**′) RAL-CHITO-41

**Table I.** BET and ZETA Characteristics for MSNs

| Sample name | B E T surface area ($m^2/g$) | BJH surface area ($m^2/g$) | Pore size (nm) | Pore volume ($cm^3/g$) | Hydrodynamic size (nm) | Zeta potential (mV) |
|---|---|---|---|---|---|---|
| MSN-41 | 713.97 | 1141.37 | 3.69 | 0.68 | 96 | −30.2 |
| RAL-41 | 394.74 | 550.23 | 3.11 | 0.29 | – | −16.5 |
| MSN-$NH_2$-41 | 529.18 | 786.92 | 3.48 | 0.67 | 112 | +12.6 |
| RAL-NH2-41 | 315.96 | 491.99 | 2.96 | 0.25 | – | +25.8 |
| MSN-CHITO-41 | 258.14 | 338.47 | 3.61 | 0.71 | 146 | +29.4 |
| RAL-CHITO-41 | 151.25 | 229.24 | 3.12 | 0.27 | – | +41.3 |

accordance with their parent value as listed in Table I. Supplementary fig. 3 demonstrated uniformity in hydrodynamic size of the constructed NPs. A single sharp and prominent peak accounted for synthesis of uniformly distributed NPs.

Furthermore, uniformity in the shape and particle size distribution was affirmed through SEM and TEM results as illustrated below in Figs. 6 and 7, respectively. Results obtained from SEM were in good agreement showing mean particle size distribution in the range between 90 to 150 nm as listed in Table I. However, the deviation of microscopy results from the DLS study results could be attributed to swollen NPs and their hydrodynamic radius as former study represented results in dry state. Apart from the uniformity in size, the internal two dimensional (2D) hexagonal arrangement for basic and modern NPs are illustrated in following Fig. 7.

## RAL Loading and Entrapment Calculation by Thermal and Spectral Analysis

As being a hydrophobic drug, RAL is having maximum solubility in organic solvent especially in MeOH. Therefore, during the drug loading, RAL was dissolved in MeOH and in this solubilized form, active drug molecule diffuses inside the mesopores through the capillaries and after solvent removal, drug remains entrapped inside the pores (36,37) . Furthermore, the DSC and WAXS data of recrystallized drug from MeOH revealed no reduction in crystallinity or in polymorphism (supplementary fig. 4A and B). %Loading capacity and %entrapment efficiency were calculated by TGA analysis (supplementary fig. 5A-D) and the UV spectrophotometric analysis. Results obtained by both analytical methods were complementary to each other and displayed 35.53, 32.15, and 34.96% (by UV) and 34.87, 31.89, and 33.57% (by TGA) %RAL loading into MSN-41, MSN-$NH_2$-41, and MSN-CHITO-41 as enumerated in Table II.

## Estimation of %Grafting of Surface-Modified MSNs

%Grafting estimation was carried out by ninhydrin and TGA analysis for amino residue attachment, whereas TGA analysis was performed for %chitosan grafting calculation. TGA study showed weight loss in two steps. The first weight loss was encountered over the range of about 25–300°C due to absorbed water or residual solvent evaporation. Whereas, second weight loss over the range of 300–700°C could be attributed to the surface phenomena indicating removal of a grafted entity from the surface (supplementary fig. 6A-C).

### *%Amine Grafting Estimation*

The Ninhydrin colorimetric assay was performed and absorbance of ninhydrin-primary amine complex was taken into consideration for the %amine grafting calculation. Colorimetric analysis of MSN-$NH_2$-41 at 590 nm showed 4.20% amine decoration on the surface of the plain MSN-41 (28). The results were calculated applying Eq. 3 and the outcome was in good agreement with that of TGA results (supplementary fig. 6A and B) Eq. 4 was taken into consideration for the %amine grafting calculation by TGA and the results showed 4.01% amine group grafting on the

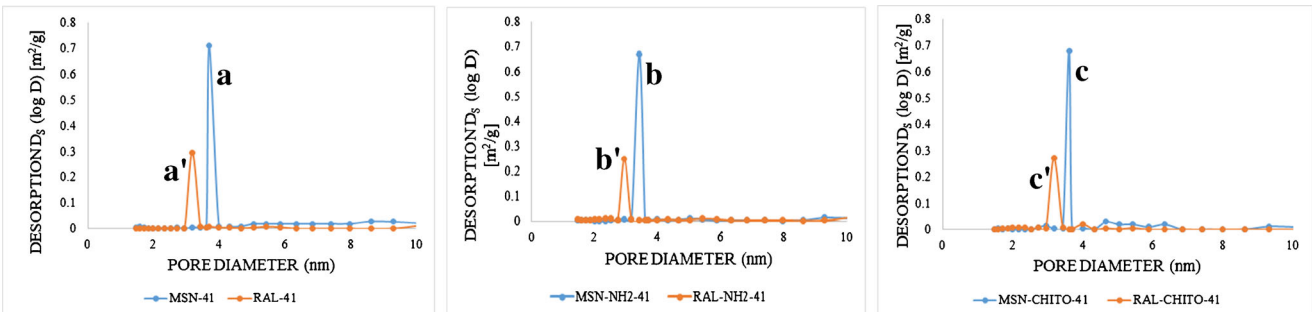


**Fig. 5.** Particle size distribution for (**a**) MSN-41 and (A') RAL-41; (**b**) MSN-$NH_2$-41 and (B′) RAL-$NH_2$–41; (**c**) MSN-CHITO-41 and (C′) RAL-CHITO-41

external surface plain NPs. Thus, the data obtained were in accordance to each other (Table III). Moreover, another parameters like $A_m$ and $A_n$ were calculated using Eqs. 1 and 2, respectively.

*%Chitosan Grafting Estimation*

A thermal method was implemented for %chitosan grafting calculation using Eq. 5. Procedure for chitosan content estimation was followed in the same manner as adopted for the estimation of %amine grafted. The results exhibited in Table III revealed 28.51% surface modification by chitosan as depicted in (supplementary 6C). Thus, larger surface area was modified with chitosan which could play a significant role in the diffusion study of same at different physiological pH (Table III).

### *In vitro* RAL Release Profile

*In vitro* study was carried out in PBS solution at three different pH viz., at 5.6, 6.8, and 7.4 representing release behavior of RAL loaded MSNs in varied pH. Figure 8 depicts the release pattern of plain RAL, RAL-41, RAL-$NH_2$-41, and RAL-CHITO-41 in PBS solution. Results demonstrated rapid release of RAL at acidic pH (pH 5.6). In contrast, release of RAL was very slow at pH 7.4. A comprehensive pH responsive study demonstrated $10.5 \pm 0.15$, $82.6 \pm 1.89$, $68.8 \pm 1.44$, and $84.2 \pm 0.98$% cumulative RAL release from plain RAL, RAL-41, RAL-$NH_2$-41, and RAL-CHITO-41 in PBS 5.6 pH. Furthermore, it was $9.9 \pm 2.16$, $80.2 \pm 1.77$, $64.1 \pm 1.05$, and $65.7 \pm 0.62$% at pH 6.8 and $9.5 \pm 1.52$, $79.9 \pm 1.69$, $62.8 \pm 1.34$, and $57.5 \pm 1.01$% at pH 7.4 respectively for RAL, RAL-41, RAL-$NH_2$-41, and RAL-CHITO-41.

### Release Kinetics Study

Release of model drug RAL favored a Korsmeyer-Peppas model to be a best fit model as it showed favorable result in terms of $r^2$ and AIC value (38). However, two different release mechanisms were envisaged for three principle nanosystems, i.e., RAL-41, RAL-$NH_2$-41, and RAL-CHITO-41. The former two systems *i.e.* release of RAL from uncoated MSN-41 and amine modified MSN-41 showed n value below 0.45. It shows that these both systems followed a Fickian diffusion mechanism, *i.e.*, the release of RAL from MSN is solely dedicated to MSN assembly. Whereas, release of RAL from chitosan grafted MSN was found to be a non Fickian release as it gave *n* value higher than 0.45. Thus, it showed that release mechanism is influence by mesopore framework and polymer swelling as well. The release pattern for decorated and undecorated NPs is summarized in Table IV.

### *In vitro* Cytotoxicity Study

To investigate the cytotoxicity effect of bare and surface functionalized NPs on MCF-7 breast carcinoma cell line, cells were treated with different concentration of NPs. Moreover, plain RAL, RAL-41, and RAL-CHITO-41, MCF-7 breast carcinoma cell line was treated with different concentration of aforementioned formulation ranging from 1 to 8 μM (concentration dependent cytotoxicity study) keeping 24 and 72 h (time dependent cytotoxicity study) incubation period. Figure 9 demonstrates the comparative cytotoxic effect of plain NPS and RAL incorporated NPs. Both RAL-41 and RAL-CHITO-41 showed a superior cytotoxic effect in contrast to plain RAL. The cytotoxicity study outcomes for MSN-41, MSN-$NH_2$-41, and MSN-CHITO-41 exhibited %relative viability $98.20 \pm 0.88$, $97.30 \pm 0.57$, and $96.40 \pm 1.02$ respectively for 24 h. Whereas, the cytotoxicity study result of 72 h revealed $97.25 \pm 0.46$, $95.59 \pm 0.64$, and $94.68 \pm 0.12$%relative cell viability for MSN-41, MSN-$NH_2$-41, and MSN-CHITO-41, respectively. Thus, it could be stated that positive charge on the external surface did not exhibit cytotoxicity on MCF-7 breast carcinoma cells. Furthermore, %relative viability calculated for RAL, RAL-41, RAL-$NH_2$-41, and RAL-CHITO-41 after 24 h incubation time were $78.89 \pm 1.22$, $42.58 \pm 0.98$, $62.18 \pm 1.44$, and $46.77 \pm 1.08$ and the figure was $70.82 \pm 1.38$, $25.67 \pm 1.55$, $31.37 \pm 1.71$, and $19.05 \pm 1.04$ after an incubation time of 72 h. Thus, the degree of cytotoxicity was solely attributed to RAL encapsulated NPs as RAL free NPs displayed > 95% relative cell viability. $IC_{50}$ values for plain RAL and RAL loaded NPs are summarized in Table V.

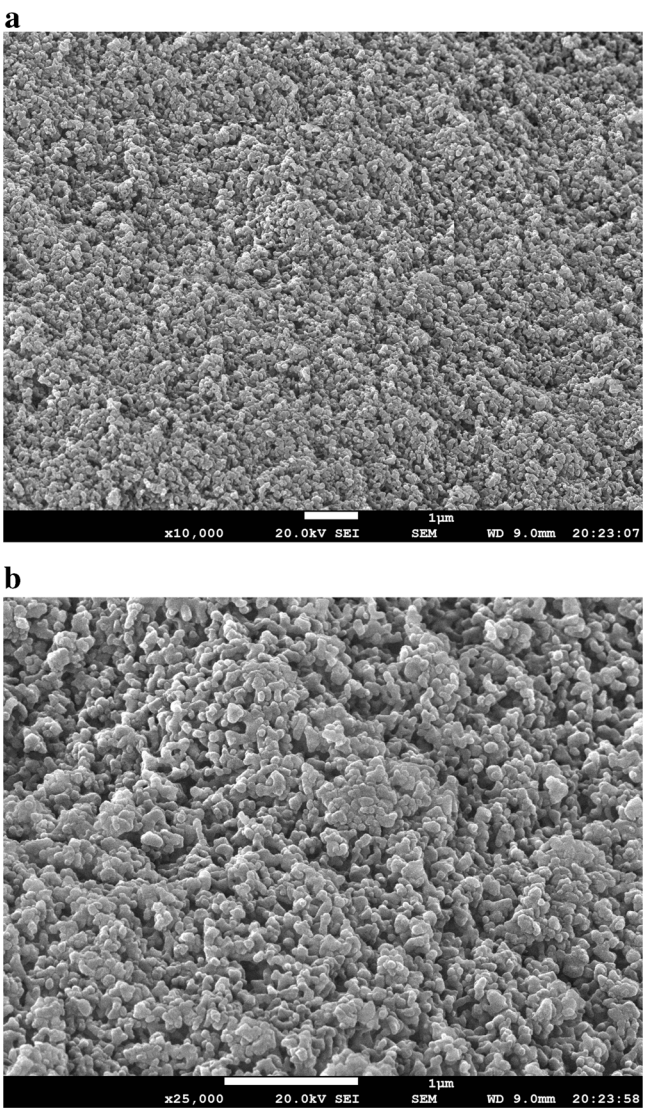


**Fig. 6.** SEM images of **a** MSN-41 and **b** MSN-CHITO-41

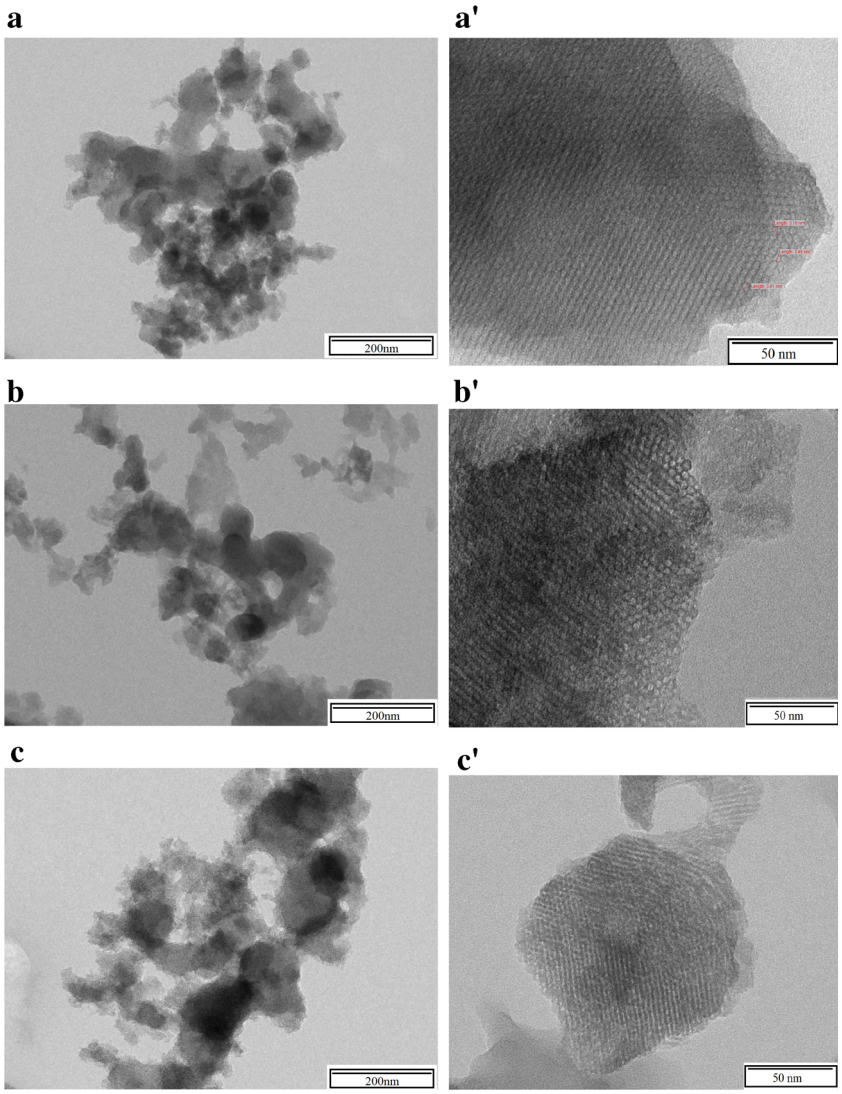


**Fig. 7.** TEM images of (**a**) MSN-41, (**b**) MSN-$NH_2$-41, and (**c**) MSN-CHITO-41 (low magnification); (**a**') MSN-41, (**b**′) MSN-$NH_2$-41, and (**c**′) MSN-CHITO-41 (high magnification)

### Hemolysis Study

Visual view of hemocompatibility of RAL loaded MSNs is provided in Fig. 10. Comparison of UV-VIS results of experimental NPs with positive control represented the maximum hemocompatibility with least hemolysis. Figure 10(A) displayed least hemolysis of RBCs in negative control. As has been positive control, the RBCs treated with 2%*v*/*v* Triton X-100 depicted significant hemolysis (Fig. 10(B)). It was clearly visible from the images that RBCs cell wall as well as shape was disturbed after Triton X-100 treatment. Identical result encountered for RAL as portrayed in Fig. 10(C) wherein RBCs structure was deformed. Wherever, the %hemolysis was negligible for RAL-41, RAL-$NH_2$-41, and RAL-CHITO-41 where the upper value of %hemolysis was $1.987 \pm 0.22$, $1.218 \pm 0.68$, and $1.153 \pm 0.49$%. Microscopic and visual view exhibiting effect of different NPs on RBC is displayed in Fig. 10(D–F). The cell wall integrity remained intake for negative control and NPs whereas the same was disturbed for plain RAL and positive control.

## DISCUSSION

The journey of this research work started with the initial step of synthesizing MSNs. The construction of MSNs begun with its basic skeletal, *i.e.*, MSN-41 which was fabricated externally to get MSN-41-$NH_2$ with ultimate MSN-CHITO-41 formation. A comprehensive BET study revealed obvious decline in surface area, pore size and pore volume from initial

**Table II.** %Loading and %Entrapment Efficiency Data

| Sample | % Loading efficiency | | % Entrapment efficiency |
|---|---|---|---|
| | UV | TGA | |
| RAL-41 | 35.53 | 34.87 | 87.5 |
| RAL-$NH_2$-41 | 32.15 | 31.89 | 80.37 |
| RAL-CHITO-41 | 34.96 | 33.57 | 86.81 |

**Table III.** %Weight Grafting Results

| Sample name | $A_m$ (mol/g) | $A_n$ (molecule/nm$^2$) | %W | |
|---|---|---|---|---|
| | | | Ninhydrin | TGA |
| MSN-$NH_2$-41 | 0.19*$10^{-3}$ | 0.2 | 4.20 | 4.01 |
| MSN-CHITO-41 | – | – | – | 28.51 |

stage (MSN-41) via intermediate stage (MSN-$NH_2$-41) and to a final destination (MSN-CHITO-41). This successive reduction could be attributed to increase in particle size after each successive modification. Furthermore, uniformity in the pore size of the manufactured NPs was envisaged by PSD and TEM outcomes and the results complemented each other. Beside pore size uniformity analysis, TEM images exhibited synthesis of ordered mesoporous framework with 2D hexagonal assembly. assembly and again this was complementary to other aforesaid investigative techniques. However, the intense deflection peak was faded after amine and chitosan attachment. MSN-$NH_2$-41 and MSN-CHITO-41 NPs were explored for %weight grafted by performing frequently employed ninhydrin colorimetric assay and thermal investigation. Significant chitosan attachment, *i.e.*, 28.51% grafting made MSN-CHITO-41 a firm base to achieve pH responsive delivery system. Inversion of zeta potential from the negative side to positive side support the formation of surface decorated NPs.

After comprehensive synthesis and characterization of NPs, model drug RAL was encapsulated inside the pore for achieving a tumor targeted delivery system. RAL incorporation was accomplished by novel technique which ensures maximum loading and entrapment efficiency. A nitrogen desorption investigation was performed and sharp reduction in surface area and the BJH pore size revealed occupation of pores by RAL. Furthermore, the existence of a hysteresis

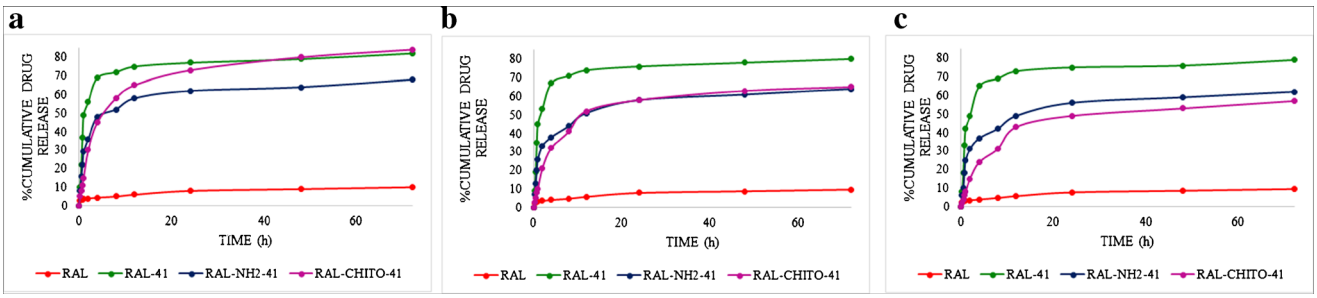


**Fig. 8.** pH responsive behaviour in three different pH **a** pH: 5.6, **b** pH: 6.8, and **c** pH: 7.4

Uniformity in particle size and increment in particle size after each modification is assigned to successive amine and chitosan grafting. In other words, with respect to particle size, MSNs ended up with healthy MSN-CHITO-41 having a particle size of 146 nm in contrast to its initial size, *i.e.*, 96 nm for pristine MSN-41 moiety. This phenomenon was assessed by SEM and hydrodynamic size investigation. Furthermore, the appearance of three distinct and characteristic deflection peaks in SAXS study revealed successive formation of mesoporous silica cycle with type IV absorption isotherm proved mesoporous structure remained unchanged after RAL loading also. Similarly, absence of prominent RAL peak appeared in FT-IR spectra of pure drug, absence of melting peak at 262.06°C in DSC thermograms, analysis of the conversion of crystalline RAL to amorphous RAL-filled NPs in WAXS investigation altogether supported the conclusion of complete uptake of RAL within the pores and ruled out the possibility of extra drug present outside the surface. Besides this, RAL occupied

**Table IV.** Release Kinetics Models

| Sample | pH | Zero order | | | First order | | | Higuchi | | | Krosmeyer-Peppas | | | |
|---|---|---|---|---|---|---|---|---|---|---|---|---|---|---|
| | | $R^2$ | $K_0$ | AIC | $R^2$ | $K_1$ | AIC | $R^2$ | $K_H$ | AIC | $R^2$ | $K_p$ | $n$ | AIC |
| MSN-41 | 5.6 | 0.819 | 2.402 | 118.560 | 0.674 | 0.404 | 97.928 | 0.290 | 16.129 | 107.252 | 0.865 | 41.214 | 0.202 | 89.305 |
| | 6.8 | 0.687 | 2.357 | 117.618 | 0.663 | 0.337 | 98.270 | 0.362 | 15.780 | 105.942 | 0.866 | 39.015 | 0.213 | 89.155 |
| | 7.4 | 0.578 | 2.313 | 116.581 | 0.642 | 0.281 | 98.772 | 0.423 | 15.424 | 104.502 | 0.873 | 37.055 | 0.223 | 88.280 |
| MSN-$NH_2$-41 | 5.6 | 0.251 | 1.926 | 109.114 | 0.317 | 0.065 | 101.840 | 0.621 | 12.580 | 94.762 | 0.933 | 27.424 | 0.254 | 75.905 |
| | 6.8 | 0.042 | 1.791 | 105.154 | 0.374 | 0.042 | 99.039 | 0.728 | 11.526 | 89.016 | 0.958 | 23.421 | 0.276 | 68.467 |
| | 7.4 | 0.037 | 1.730 | 103.845 | 0.405 | 0.038 | 98.061 | 0.756 | 11.098 | 87.355 | 0.952 | 21.801 | 0.287 | 69.869 |
| MSN-CHITO-41 | 5.6 | 0.434 | 2.310 | 106.843 | 0.888 | 0.097 | 87.341 | 0.892 | 14.461 | 86.973 | 0.942 | 12.107 | 0.458 | 81.333 |
| | 6.8 | 0.514 | 1.798 | 99.452 | 0.779 | 0.039 | 90.001 | 0.915 | 11.167 | 78.470 | 0.946 | 15.715 | 0.494 | 75.094 |
| | 7.4 | 0.549 | 1.456 | 93.810 | 0.736 | 0.025 | 87.388 | 0.921 | 9.005 | 72.898 | 0.942 | 21.997 | 0.489 | 71.069 |

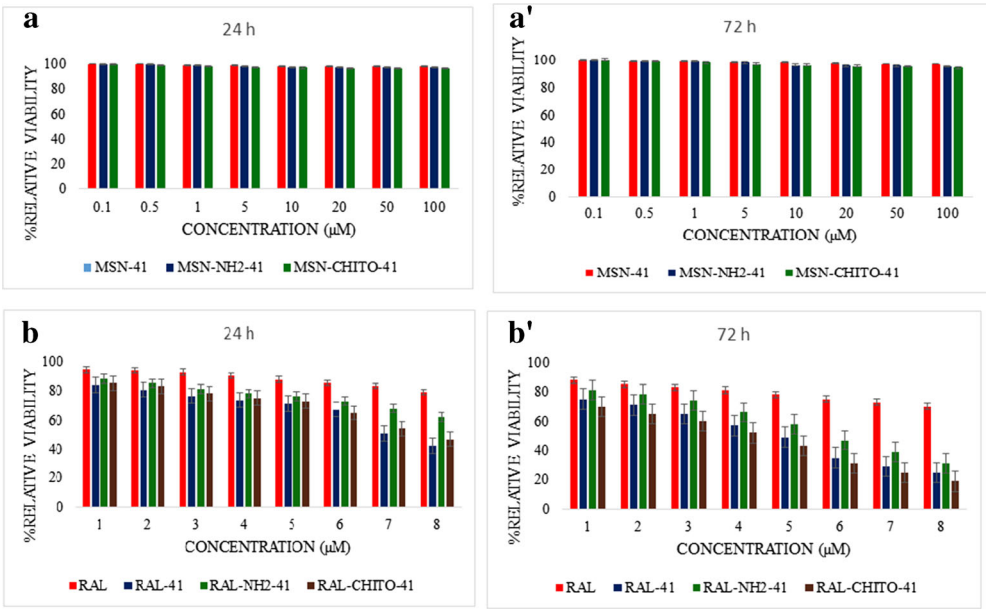


**Fig. 9.** Cytotoxicity for MSN-41, MSN-$NH_2$-41 and MSN-CHITO-41 against MCF-7 evaluated at (**a**) 24 and (**a**') 72 h; RAL, RAL-41, RAL-$NH_2$-41, and RAL-CHITO-41 against MCF-7 evaluated at (**b**) 24 and (**b**′) 72 h

NPs were subjected to SEM, TEM, DLS analysis to confirm uniformity in particle size, pore size distribution and to check the integrity of the internal hexagonal structure after RAL encapsulation.

Furthermore *in vitro* release study for NPs was employed at three different pH of PBS solution to envisage pH dependent release behaviour of RAL-CHITO-41 nanosystem. Diffusion data revealed the higher RAL release from RAL-CHITO-41 at acidic pH which was dedicated to unique property of chitosan which swells at acidic pH following the pore opening which leads to higher drug release in an acidic environment (39). In contrast, chitosan gets collapsed after moving away from acidic pH. This resulted into film formation, which covered the pores and ultimately exhibited significant fall in RAL release at higher pH. However, drug release from RAL-CHITO-41 was slower as compared to RAL-41 till 24 h which could be allocated to chitosan's polymer property. However, RAL release was equivalent after 72 h from CHITO-41 as compared to MSN-41. This phenomenon is solely attributed to unique pH responsive property of chitosan. Thus, being a polymer, chitosan provided controlled release of RAL with the evident pH selective release. Maximum RAL release from RAL-CHITO-41 in PBS-5.6 was achieved within 72 h. Thus, pH responsive NPs were successfully fabricated to direct the drug release exclusively to cancer cells. Apart from rate of release at different PBS pH, the outcomes of release mechanism study favored Krosmeyer-Peppas model as it showed supreme results with respect to $R^2$ and AIC variables for all three pH of PBS solution. Additionally, controversy between Fickian and non-Fickian type of release mechanism for amine and chitosan decorated MSN correspondingly was explored to the depth (30,40). For basic (RAL-41) and amine coated NPs (RAL-$NH_2$-41), the release was solely due to the NP system and therefore, it was obvious that it should follow non-Fickian release mechanism and this was also proved practically by statistical analysis. As stated earlier, chitosan grafted nanosystem showed RAL release in a controlled manner which was because of polymeric property of chitosan and silica NPs system also play a vital role in RAL release. Thus, latter two phenomenon worked simultaneously and showed *n* values greater than 0.45 for MSN-CHITO-41, hence it showed anomalous release mechanism.

Furthermore, the MTT cell viability assay performed on human breast cancer cell line MCF-7 for drug encapsulated NPs results showed significant cytotoxicity of RAL-41 and RAL-CHITO-41 towards MCF-7 breast cancer cells in time dependent and concentration dependent manner. MTT assay exhibited less %relative viability for RAL-41 compared to RAL-CHITO-41 after 24 h incubation time period. This results were complementary to the diffusion release data of RAL where, %RAL release was higher from RAL-41 with respect to RAL-CHITO-41 in acidic diffusion media. However, %relative viability was almost equivalent for both of the formulation by imparting 72 h incubation treatment to MCF-7 cells. Again here, diffusion data favors the aforesaid statement as an identical RAL release was achieved for both nanoparticulate systems after 72 h. This outcome supported the selective and pH responsive behavior of RAL-CHITO-41 NPs. Moreover, the $IC_{50}$ values for pure RAL were higher as compared to RAL-41. The $IC_{50}$ values were beyond 8 μM for RAL after 72 h incubation time. The values were 7.16 ± 0.12 and 7.53 ± 0.56 μM for RAL-41 and RAL-CHITO-41 correspondingly

**Table V.** $IC_{50}$ Values for RAL Nanoparticles

| Time (h) | Concentration with respect to $IC_{50}$ (μM)* | | | |
|---|---|---|---|---|
| | RAL | RAL-41 | RAL-$NH_2$-41 | RAL-CHITO-41 |
| 24 | > 8 | 7.16 ± 0.12 | > 8 | 7.53 ± 0.56 |
| 72 | > 8 | 4.86 ± 0.75 | 5.67 ± 0.23 | 4.27 ± 0.89 |

*The study was conducted in three replicates and results were displayed in mean ± S.D.

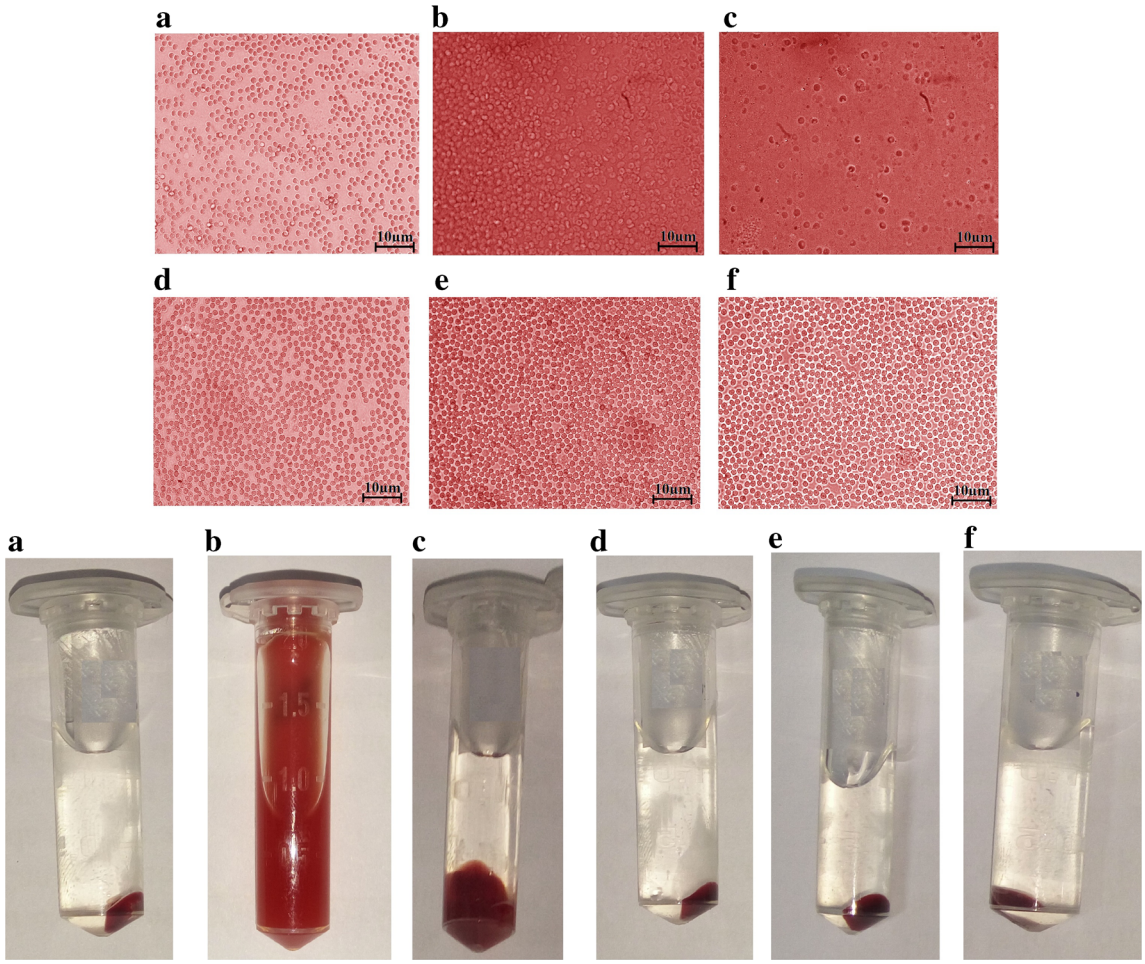


**Fig. 10.** Microscopic and visual images for (**a**) negative control, (**b**) positive control, (**c**) RAL, (**d**) RAL-41, (**e**) RAL-$NH_2$-41, (**f**) RAL-CHITO-41

estimated after 24 h incubation period, whereas the values were 4.86 ± 0.75, 5.67 ± 0.23, and 4.27 ± 0.89 μM for RAL-41, RAL-$NH_2$-41, and RAL-CHITO-41 respectively after 72 h incubation time. Thus, lower $IC_{50}$ values for RAL-41 with respect to pure RAL suggested the greater cytotoxic potential of former to cancer cells. Additionally, lowest $IC_{50}$ value after 72 h for RAL-CHITO-41 displayed control and pH responsive nature of chitosan coated nano assembly which would efficiently and selectively release the anticancer moiety in a time dependent manner. Moreover, biosafety and hemocompatibility study of NP revealed significant biosafety with %hemolysis of below 5% for each formulation, which falls within the acceptance criteria (< 5%) and again it proved to be biologically safe and hemocompatible.

## CONCLUSIONS

Present work involved synthesis of bare and chitosan coated MSNs where amine functionalized MSNs served as a base for external surface modification. Our findings confirmed the application of chitosan coated NP system as a pH responsive carrier for selective RAL release in acidic environment *i.e.* into tumor cells along with controlled release. Additionally, surface modified MSNs were found to be biosafe and hemocompatible. Thus, they can be successfully employed as pH responsive controlled drug release system with exclusive cancer cell targeted release system along with least off site side effects. We believe that our finding will make pharma world more familiar with advantage and application of chitosan based NPs for targeted cancer treatment.

## ACKNOWLEDGEMENTS

The authors thank Dr. Amirali Popat, School of Pharmacy, The University of Queensland, Australia and Zydus research centre, Gujarat, India for providing RAL gift sample.

## COMPLIANCE WITH ETHICAL STANDARDS

**Conflict of Interest** The authors declare that they have no conflict of interest.

## REFERENCES

1. Daryasari MP, Akhgar MR, Mamashli F, Bigdeli B, Khoobi M. Chitosan-folate coated mesoporous silica nanoparticles as a smart and pH-sensitive system for curcumin delivery. RSC Adv. 2016;6(107):105578–88. https://doi.org/10.1039/C6RA23182A.

2. de Oliveira Freitas LB, Bravo IJG, de Almeida Macedo WA, de Sousa EMB. Mesoporous silica materials functionalized with folic acid: preparation, characterization and release profile study with methotrexate. J Sol-Gel Sci Technol. 2016;77(1):186–204. https://doi.org/10.1007/s10971-015-3844-8.
3. Maleki A, Hamidi M. Dissolution enhancement of a model poorly water-soluble drug, atorvastatin, with ordered mesoporous silica: comparison of MSF with SBA-15 as drug carriers. Expert Opin Drug Deliv. 2016;13(2):171–81. https://doi.org/10.1517/17425247.2015.1111335.
4. Anirudhan T, Binusreejayan, Jayan PP. Development of functionalized chitosan-coated carboxylated mesoporous silica: a dual drug carrier. Des Monomers Polym. 2016;19(5):381–93.
5. Tang F, Li L, Chen D. Mesoporous silica nanoparticles: synthesis, biocompatibility and drug delivery. Adv Mater. 2012;24(12):1504–34. https://doi.org/10.1002/adma.201104763.
6. Vadia N, Rajput S. Study on formulation variables of methotrexate loaded mesoporous MCM-41 nanoparticles for dissolution enhancement. Eur J Pharm Sci. 2012;45(1):8–18. https://doi.org/10.1016/j.ejps.2011.10.016.
7. Ganesh M, Ubaidulla U, Hemalatha P, Peng MM, Jang HT. Development of duloxetine hydrochloride loaded mesoporous silica nanoparticles: characterizations and in vitro evaluation. AAPS PharmSciTech. 2015;16(4):944–51. https://doi.org/10.1208/s12249-014-0273-x.
8. Bharti C, Nagaich U, Pal AK, Gulati N. Mesoporous silica nanoparticles in target drug delivery system: a review. Int J Pharm Investig. 2015;5(3):124–33. https://doi.org/10.4103/2230-973X.160844.
9. Roggers R, Kanvinde S, Boonsith S, Oupický D. The practicality of mesoporous silica nanoparticles as drug delivery devices and progress toward this goal. AAPS PharmSciTech. 2014;15(5):1163–71. https://doi.org/10.1208/s12249-014-0142-7.
10. Gulfam M, Chung BG. Development of pH-responsive chitosan-coated mesoporous silica nanoparticles. Macromol Res. 2014;22(4):412–7. https://doi.org/10.1007/s13233-014-2063-4.
11. Wu X, Wang Z, Zhu D, Zong S, Yang L, Zhong Y, et al. pH and thermo dual-stimuli-responsive drug carrier based on mesoporous silica nanoparticles encapsulated in a copolymer–lipid bilayer. ACS Appl Mater Interfaces. 2013;5(21):10895–903. https://doi.org/10.1021/am403092m.
12. Lim E-K, Sajomsang W, Choi Y, Jang E, Lee H, Kang B, et al. Chitosan-based intelligent theragnosis nanocomposites enable pH-sensitive drug release with MR-guided imaging for cancer therapy. Nanoscale Res Lett. 2013;8(1):467. https://doi.org/10.1186/1556-276X-8-467.
13. Hu X, Wang Y, Peng B. Chitosan-capped mesoporous silica nanoparticles as pH-responsive nanocarriers for controlled drug release. Chem Asian J. 2014;9(1):319–27.
14. Ahmadi Nasab N, Hassani Kumleh H, Beygzadeh M, Teimourian S, Kazemzad M. Delivery of curcumin by a pH-responsive chitosan mesoporous silica nanoparticles for cancer treatment. Artif Cells Nanomed Biotechnol. 2017:1–7. https://doi.org/10.1080/21691401.2017.1290648.
15. Lv G, Qiu L, Liu G, Wang W, Li K, Zhao X, et al. pH sensitive chitosan-mesoporous silica nanoparticles for targeted delivery of a ruthenium complex with enhanced anticancer effects. Dalton Trans. 2016;45(45):18147–55. https://doi.org/10.1039/C6DT03783F.
16. Peng H, Dong R, Wang S, Zhang Z, Luo M, Bai C, et al. A pH-responsive nano-carrier with mesoporous silica nanoparticles cores and poly (acrylic acid) shell-layers: fabrication, characterization and properties for controlled release of salidroside. Int J Pharm. 2013;446(1):153–9. https://doi.org/10.1016/j.ijpharm.2013.01.071.
17. Yuan L, Tang Q, Yang D, Zhang JZ, Zhang F, Hu J. Preparation of pH-responsive mesoporous silica nanoparticles and their application in controlled drug delivery. J Phys Chem C. 2011;115(20):9926–32. https://doi.org/10.1021/jp201053d.
18. Tang H, Guo J, Sun Y, Chang B, Ren Q, Yang W. Facile synthesis of pH sensitive polymer-coated mesoporous silica nanoparticles and their application in drug delivery. Int J Pharm. 2011;421(2):388–96. https://doi.org/10.1016/j.ijpharm.2011.10.013.
19. Li G, Liu G, Kang E, Neoh K, Yang X. pH-responsive hollow polymeric microspheres and concentric hollow silica microspheres from silica− polymer core− shell microspheres. Langmuir. 2008;24(16):9050–5. https://doi.org/10.1021/la8010579.
20. Gulzar A, Gai S, Yang P, Li C, Ansari MB, Lin J. Stimuli responsive drug delivery application of polymer and silica in biomedicine. J Mater Chem B. 2015;3(44):8599–622. https://doi.org/10.1039/C5TB00757G.
21. Jordan V. Beyond raloxifene for the prevention of osteoporosis and breast cancer. Br J Pharmacol. 2007;150(1):3–4. https://doi.org/10.1038/sj.bjp.0706962.
22. Jha RK, Tiwari S, Mishra B. Bioadhesive microspheres for bioavailability enhancement of raloxifene hydrochloride: formulation and pharmacokinetic evaluation. AAPS PharmSciTech. 2011;12(2):650–7. https://doi.org/10.1208/s12249-011-9619-9.
23. Rampino A, Borgogna M, Blasi P, Bellich B, Cesàro A. Chitosan nanoparticles: preparation, size evolution and stability. Int J Pharm. 2013;455(1):219–28. https://doi.org/10.1016/j.ijpharm.2013.07.034.
24. Woraphatphadung T, Sajomsang W, Gonil P, Treetong A, Akkaramongkolporn P, Ngawhirunpat T, et al. pH-responsive polymeric micelles based on amphiphilic chitosan derivatives: effect of hydrophobic cores on oral meloxicam delivery. Int J Pharm. 2016;497(1):150–60. https://doi.org/10.1016/j.ijpharm.2015.12.009.
25. Shah PV, Rajput SJA. Comparative in vitro release study of raloxifene encapsulated ordered MCM-41 and MCM-48 nanoparticles: a dissolution kinetics study in simulated and biorelevant media. J Drug Delivery Sci Technol. 2017;41:31–44. https://doi.org/10.1016/j.jddst.2017.06.015.
26. Wouters BH, Chen T, Dewilde M, Grobet PJ. Reactivity of the surface hydroxyl groups of MCM-41 towards silylation with trimethylchlorosilane. Microporous Mesoporous Mater. 2001;44:453–7.
27. Ebrahimi-Gatkash M, Younesi H, Shahbazi A, Heidari A. Amino-functionalized mesoporous MCM-41 silica as an efficient adsorbent for water treatment: batch and fixed-bed column adsorption of the nitrate anion. Appl Water Sci 2015:1–15.
28. Yoncheva K, Popova M, Szegedi A, Mihály J, Tzankov B, Lambov N, et al. Functionalized mesoporous silica nanoparticles for oral delivery of budesonide. J Solid State Chem. 2014;211:154–61. https://doi.org/10.1016/j.jssc.2013.12.020.
29. Rosen JE, Surface GFX. Functionalization of silica nanoparticles with cysteine: a low-fouling zwitterionic surface. Langmuir. 2011;27(17):10507–13. https://doi.org/10.1021/la201940r.
30. Ding Y, Shen SZ, Sun H, Sun K, Liu F, Qi Y, et al. Design and construction of polymerized-chitosan coated Fe 3 O 4 magnetic nanoparticles and its application for hydrophobic drug delivery. Mater Sci Eng C. 2015;48:487–98. https://doi.org/10.1016/j.msec.2014.12.036.
31. Lu H-T. Synthesis and characterization of amino-functionalized silica nanoparticles. Colloid J. 2013;75(3):311–8.
32. de Oliveira LFA, Bouchmella K, KDA G, Bettini J, Kobarg J, Cardoso MB. Functionalized silica nanoparticles as an alternative platform for targeted drug-delivery of water insoluble drugs. Langmuir. 2016;32(13):3217–25. https://doi.org/10.1021/acs.langmuir.6b00214.
33. Zhao Y, Sun X, Zhang G, Trewyn BG, Slowing II, Lin VS-Y. Interaction of mesoporous silica nanoparticles with human red blood cell membranes: size and surface effects. ACS Nano. 2011;5(2):1366–75. https://doi.org/10.1021/nn103077k.
34. Akrami M, Khoobi M, Khalilvand-Sedagheh M, Haririan I, Bahador A, Faramarzi MA, et al. Evaluation of multilayer coated magnetic nanoparticles as biocompatible curcumin delivery platforms for breast cancer treatment. RSC Adv. 2015;5(107):88096–107. https://doi.org/10.1039/C5RA13838H .
35. Li J, Zheng L, Cai H, Sun W, Shen M, Zhang G, et al. Polyethyleneimine-mediated synthesis of folic acid-targeted iron oxide nanoparticles for in vivo tumor MR imaging. Biomaterials. 2013;34(33):8382–92. https://doi.org/10.1016/j.biomaterials.2013.07.070.
36. Charnay C, Bégu S, Tourné-Péteilh C, Nicole L, Lerner D, Devoisselle J-M. Inclusion of ibuprofen in mesoporous templated silica: drug loading and release property. Eur J Pharm Biopharm. 2004;57(3):533–40. https://doi.org/10.1016/j.ejpb.2003.12.007.
37. Patil A, Chirmade U, Trivedi V, Lamprou D, Urquart A, Douroumis D. Encapsulation of water insoluble drugs in mesoporous silica nanoparticles using supercritical carbon dioxide. Journal of Nanomedicine and Nanotechnology 2011;2(3).

38. Carriazo D, Del Arco M, Fernández A, Martín C, Rives V. Inclusion and release of fenbufen in mesoporous silica. J Pharm Sci. 2010;99(8):3372–80. https://doi.org/10.1002/jps.22096.
39. Mahdavinia G, Pourjavadi A, Hosseinzadeh H, Zohuriaan M. Modified chitosan 4. Superabsorbent hydrogels from poly (acrylic acid-co-acrylamide) grafted chitosan with salt-and pH-responsiveness properties. Eur Polym J. 2004;40(7):1399–407. https://doi.org/10.1016/j.eurpolymj.2004.01.039.
40. Tan D, Yuan P, Annabi-Bergaya F, Liu D, Wang L, Liu H, et al. Loading and in vitro release of ibuprofen in tubular halloysite. Appl Clay Sci. 2014;96:50–5. https://doi.org/10.1016/j.clay.2014.01.018.
41. Seema Saroj, Sadhana J. Rajput, (2018) Etoposide encapsulated functionalized mesoporous silica nanoparticles: Synthesis, characterization and effect of functionalization on dissolution kinetics in simulated and biorelevant media. J Drug Delivery Sci Technol 44:27–40.